Infrared reflectivity of $Tl_{1.94}Mn_2O_{6.96}$

Néstor E. Massa*
Laboratorio Nacional de Investigación y Servicios en Espectroscopía Optica, Centro CEQUINOR–Departamento de Química and Departamento de Física, Universidad Nacional de La Plata, C.C. 962, 1900 La Plata, Argentina

José Antonio Alonso, María Jesús Martínez-Lope, and María Teresa Casais
Instituto de Ciencia de Materiales de Madrid, Consejo Superior de Investigaciones Científicas, Cantoblanco, E-28049 Madrid, Spain

Horacio Salva
Comisión Nacional de Energía Atómica, Centro Atómico Bariloche and Instituto Balseiro, 8400 Bariloche, Rio Negro, Argentina
(Received 19 August 1998; revised manuscript received 24 February 1999)

We report temperature dependent infrared reflectivity of $Tl_{1.94}Mn_2O_{6.96}$ in the 30 to 10 000 cm^{-1} frequency range. We found that between room temperature and the Curie temperature ($T_C \cong T_{IM}$) in which the insulator-ferromagnetic metal phase transition takes place, $Tl_{1.94}Mn_2O_{6.96}$ behaves as an insulator with antiresonances near the longitudinal optical modes indicating distinctive electron-phonon interactions. Below T_C the band envelope assigned to breathing oxygen phonons undergoes broadening and frequency hardening and the sample becomes a poor metal oxide in which small trapped polaron electrons are released with decreasing temperature. We support this conclusion pointing to the agreement between the experimental and the calculated; using Reik's small polaron theory, optical conductivity strongly suggests that conductivity be achieved by phonon assisted electron hopping. [S0163-1829(99)06833-2]

INTRODUCTION

$Tl_2Mn_2O_7$ is unique among manganese pyrochlores in the sense that it simultaneously exhibits ferromagnetic ordering and metallic behavior below a characteristic Curie temperature (T_C), and shows colossal magnetoresistance (CMR) at temperatures close to T_C. Here we discuss the results of an infrared reflectivity study for $Tl_2Mn_2O_7$ as the amount of mobile carriers increases below T_C and then compare with the overall features that have been found in the most widely studied manganese perovskites exhibiting CMR (e.g., $La_{0.7}A_{0.3}MnO_3$; *A*: alkaline earths).

In common with manganese perovskites, face centered cubic pyrochlores also contain a corner-sharing sublattice of manganese octahedra. In fact, the pyrochlore structure, of general stoichiometry $A_2B_2O_6O'$, can be described as two interpenetrating networks: the smaller *B* cations (e.g., Mn in $Tl_2Mn_2O_7$) are octahedrally coordinated to O-type oxygens, the BO_6 octahedra sharing corners to give a B_2O_6 sublattice, which can be considered as the backbone of the structure. The cagelike holes of this network contain a second sublattice A_2O', not essential for the stability of the structure.[1] ''*A*'' atoms are in a pseudocubic environment. Whereas in manganese perovskites the Mn-O-Mn angle is about 160°, in the B_2O_6 sublattice of pyrochlores the *B*-O-*B* angle is in the range 130°–140°.

In mixed-valence manganese perovskites, the role of a strong electron-phonon coupling has been demonstrated to be essential in explaining the magnetotransport properties of these mixed-valence systems. In systems like $(La^{3+}_{0.7}Sr^{2+}_{0.3})MnO_3$ [containing 70%(Mn^{3+})–30%(Mn^{4+})] the carrier localization is minimized at and below T_C by a double exchange mechanism[2] accounting for both the ferromagnetic ordering below T_C (Ref. 3) and the metallic conductivity. The ferromagnetic transition temperature in ^{16}O and ^{18}O isotope substituted manganites shifts as a consequence of the strong coupling of local carriers to Jahn-Teller distortions giving clues on the existence of magnetic polarons.[4] To explain the colossal magnetoresistance in these compounds dynamic Jahn Teller effect was then put forward by Millis *et al.*[5] in addition to Zener's double exchange mechanism,[2] in which the strong electron-phonon interaction is taken into account in a mean field approximation.

By contrast, in $Tl_2Mn_2O_7$ pyrochlore the absence of any structural anomaly associated with the change in magnetotransport properties at T_C had suggested weak spin-lattice and charge lattice correlations,[6] which is further supported by the apparent absence of Jahn-Teller distortions of the MnO_6 octahedra, from diffraction data,[7] in the undistorted cubic pyrochlore structure. However, from our infrared reflectivity data we give evidence on the existence of distinctive electron-phonon interactions in $Tl_2Mn_2O_7$, showing that conductivity is achieved by phonon assisted electron hopping.

SAMPLE PREPARATION AND CHARACTERIZATION

A sample of nominal composition $Tl_2Mn_2O_7$ was prepared under high-pressure conditions. About 1.5 g of a stoichiometric mixture of Tl_2O_3 and MnO_2 oxides were thoroughly ground and put into a gold capsule (8 mm diam), sealed and placed in a cylindrical graphite heater. The reaction was carried out in a piston-cylinder press (Rockland Research Co.), at a pressure of 20 kbar at 1000 °C for 20 min. Then the materials were quenched to room temperature and the pressure was subsequently released. The reaction products were characterized by x-ray diffraction (XRD): all the patterns corresponded to single phased pyrochlores.[8] All

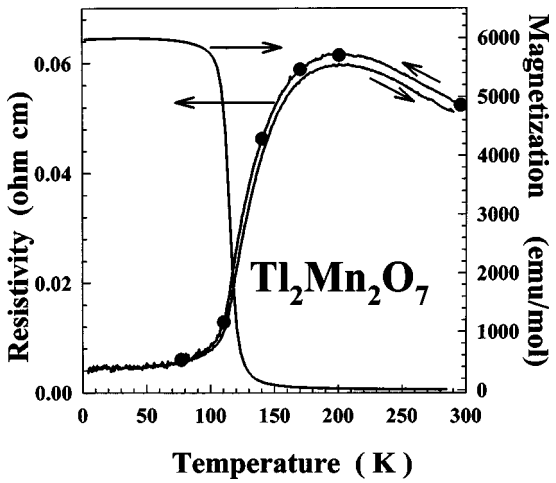

FIG. 1. Temperature dependent resistivity and susceptibility (measured at 500 G) of $Tl_{1.94}Mn_2O_{6.96}$. Dots signal the temperatures at which the reflectivity was measured.

reflections could be indexed in a cubic unit cell, with **a** $=9.8909(1)$ Å. Because the XRD scattering factors of Tl and Mn are considerably higher than that of oxygen we have also used neutron diffraction patterns (NPD) collected at room temperature on the high resolution D2B diffractometer at the Institut Laue-Langevin, Grenoble, with a wavelength $\lambda = 1.594$ Å. The crystal structure was refined in the cubic space group Fd-3m (No. 227) with eight formula units per unit cell.[9,10,11] This yielded accurate structural information concerning metal-to-oxygen distances and Mn-O-Mn angles. The Mn-O distance observed for $Tl_2Mn_2O_7$, is 1.9000(4) Å. Mn-O-Mn angles are 134.09(3)° consistent with the reported values by Shimakawa *et al.*[7] The refinement of the occupancy factor of Tl and O′ lead to a slightly defective crystallographic stoichiometry of $Tl_{1.944(6)}Mn_2O_6O'_{0.96(1)}$. Tl vacancies (in a concentration of 2.8%) are accompanied by O′ vacancies in such a way that a formal valence of +4.05(4) is obtained for Mn (assuming trivalent Tl cations and divalent O anions), close to the expected value of +4 (Ref. 11).

Pellets of $Tl_{1.94}Mn_2O_{6.96}$ suitable for reflectivity measurements were mechanically polished to obtain a shiny surface. As-grown material, diluted in CsI or polyethylene, was also used in transmission measurements to verify the main features temperature dependence in the spectral range of this study. Infrared spectra, with 2 and 4 cm^{-1} resolution, were taken between 30 and 10000 cm^{-1} in a Bruker 113 v FTIR spectrometer with samples mounted in the cold finger of a DN 1754 Oxford cryostat. Magnetization was measured with a Quantum Design SQUID magnetometer under 500 G with samples of 4.25 mg. Four point resistivity measurements of same batch samples were performed between 4 and 300 K. Shown in Fig. 1, they agree with those reported by Cheong *et al.*,[12] the drop in resistivity associated with the ferromagnetic transition. We do not observe the anomalous resistivity upturn reported by Shimakawa *et al.*[7] between 225 and 300 K. The dots in Fig. 1 signal the temperatures at which the reflectivity was measured.

SPECTRAL ANALYSIS

We estimated phonon frequencies using a standard multioscillator dielectric simulation fit of our reflectivity spectra.[13] Thus, $\varepsilon(\omega)$, the dielectric function, is given by

$$\varepsilon(\omega)=\varepsilon_1(\omega)+i\varepsilon_2(\omega)=\varepsilon_\infty\prod_j\frac{(\Omega_{j\mathrm{LO}}^2-\omega^2+i\gamma_{j\mathrm{LO}}\omega)}{(\Omega_{j\mathrm{TO}}^2-\omega^2+i\gamma_{j\mathrm{TO}}\omega)}. \tag{1}$$

We then optimized the normal reflectivity against the experimental points and calculated the high frequency dielectric function, ϵ_∞, the transverse and longitudinal jth optical frequencies, $\Omega_{j\mathrm{TO}}$ and $\Omega_{j\mathrm{LO}}$, and their transverse and longitudinal damping constants, $\gamma_{j\mathrm{TO}}$ and $\gamma_{j\mathrm{LO}}$, respectively. We also calculated the S_j strength of the jth oscillator as

$$S_j=\Omega_{j\mathrm{TO}}^{-2}\frac{\left(\prod_k\Omega_{k\mathrm{LO}}^2-\Omega_{j\mathrm{TO}}^2\right)}{\left(\prod_{k\neq j}\Omega_{k\mathrm{TO}}^2-\Omega_{j\mathrm{TO}}^2\right)}. \tag{2}$$

In addition, when the measured spectra required it, we added the plasma contribution (Drude term) as

$$-\frac{[\Omega_{\mathrm{pl}}^2+i(\gamma_{\mathrm{pl}}-\gamma_0)\omega]}{[\omega(\omega-i\gamma_0)]} \tag{3}$$

to the dielectric simulation function, where Ω_{pl} is the plasma frequency, γ_{pl} its damping, and γ_0 is understood as a phenomenological damping introduced by the lattice drag. When these two damping are set equal, one retrieves the classical Drude formula.[14]

With

$$\Omega_{\mathrm{pl}}^2=4\pi e^2N/m^*, \tag{4}$$

we estimate an effective carrier concentration $N^*=Nm_0/m^*$ (m_0 and m^* are the free and effective electron mass; N and N^* are the number and the effective number of carriers, respectively).

To study the real part of the optical conductivity, $\sigma_1=(\omega/4\pi)\varepsilon_2$ (ε_2 is the imaginary part of the dielectric function), we used theoretical expressions for small polarons due to non-diagonal phonon transitions calculated by Reik and Heese.[15,16] The frequency dependent conductivity is calculated using Kubo's[17] formula starting with a Holstein's Hamiltonian.[18] In this model optical properties are due to carriers in one small band and interband transition are excluded. The real part of the conductivity $\sigma_1(\omega,\beta)$ for finite temperature is given by

$$\sigma_1(\omega,\beta)=\sigma_{\mathrm{dc}}\frac{\sinh\left(\frac{1}{2}\hbar\omega\beta\right)\exp[-\omega^2\tau^2r(\omega)]}{\frac{1}{2}\hbar\omega\beta[1+(\omega\tau\Delta)^2]^{1/4}}, \tag{5}$$

where

$$r(\omega)=\left(\frac{2}{\omega\tau\Delta}\right)\ln\{\omega\tau\Delta+[1+(\omega\tau\Delta)^2]^{1/2}\}-\left[\frac{2}{(\omega\tau\Delta)^2}\right]\{[1+(\omega\tau\Delta)^2]^{1/2}-1\}, \tag{6}$$

with

$$\Delta=2\bar{\omega}\tau \tag{7}$$

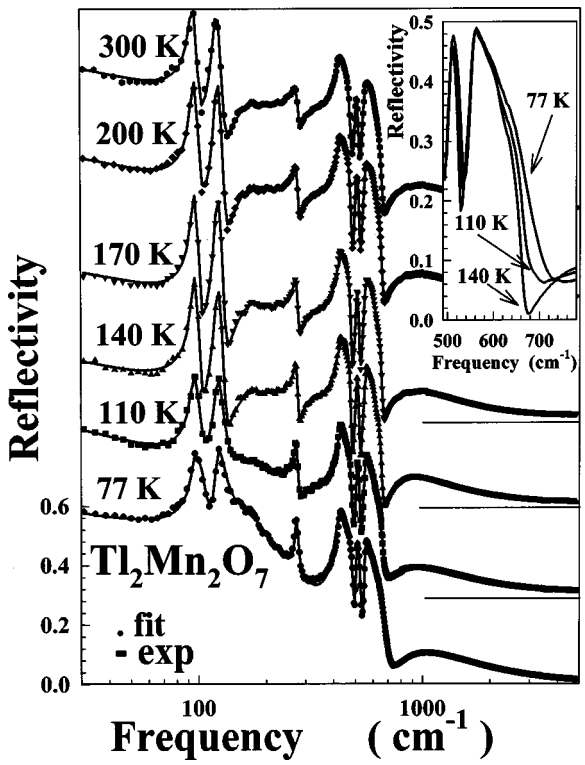

FIG. 2. Temperature dependent reflectivity of $Tl_{1.94}Mn_2O_{6.96}$. Dots: experimental; full lines: fitted. The inset shows the behavior of the band assigned to octahedra oxygen breathing modes at the insulator-metal transition.

and

$$\tau^2=\left[\sinh\left(\frac{1}{2}\hbar\bar{\omega}\beta\right)\right]\Big/\ 2\bar{\omega}^2\eta. \tag{8}$$

$\sigma_{dc}=\sigma(\omega=0,\beta)$ is the electrical conductivity (taken from our resistivity measurements, Fig. 1) and $\beta=1/kT$. The frequency $\bar{\omega}$ corresponds to the average between the transverse and the longitudinal optical mode of a reststrahlen band and η, characterizing the strength of the electron-phonon interaction, is the average number of phonons that contribute to the polarization around a localized polaron.[19] Thus, since phonon frequencies are fixed by reflectivity measurements, the only remaining parameter free to fit in each phonon contribution is η.

REFLECTIVITIES AND DISCUSSION

Figure 2 shows the reflectivity spectra of $Tl_{1.94}Mn_2O_{6.96}$ at 300, 200, 170, 140, 110, and 77 K. The room temperature spectrum closely corresponds to one for a dielectric material in which every phonon band has an antiresonance near a longitudinal optical mode thus denoting distinctive electron-phonon interactions. We understand the bands as envelopes of the different vibrational modes of $Tl_2Mn_2O_7$ that in the dielectric simulation count to a minimum of eleven oscillators (Table I). In addition we add an extra one to take into account the feature centered between $\sim$700 and 1200 cm^{-1} assigned to polaron formation. At temperatures above T_C we found no need to introduce a Drude term.

As it was pointed out in the Introduction, octahedra and pseudocubic cages build a pyrochlore lattice. The manganese ions are in six oxygen-coordinated octahedra similar to those in perovskite manganites. Thus, although the Mn-O-Mn angles are different, we expect that the internal vibrational modes, symmetric (breathing) and antisymmetric stretching, be close to the frequencies found in those systems and in agreement with the general assignment for the cubic perovskite structure. In addition, the ion mass (Tl ions are heavier than Mn ions), determines that the band at highest frequency, $\sim$600 cm^{-1}, be identified in the pyrochlore structure as for breathing Mn octahedra. Then, octahedral (Mn) and pseudocubic (Tl) symmetric stretching breathing modes are assigned in the spectral region between 660 and 542 cm^{-1}. Similar analysis leads us to identify bending deformation antisymmetric modes between 500 and 161 cm^{-1} and lattice modes at 130 and 93 cm^{-1}. This is also supported by observing that in the mixed pyrochlore $Tl_{1.5}Bi_{0.5}Mn_2O_7$, Bi replacing Tl ions, bands below $\sim$500 cm^{-1} change in shape and relative strength but the assignment to the octahedral breathing modes is not modified.[20]

From ambient temperature to 140 K the spectra do not change significantly other than in damping of the transverse and longitudinal optical modes. As shown in Fig. 3 the bands peak positions are not affected as the temperature is varied. The exception to this behavior is octahedral modes. The oxygens breathing band, at 634–660 cm^{-1}, softens between 300 and 110 K and hardens and broadens (inset, Fig. 2 and Fig. 3) below this temperature implying a significant role of these phonons in the insulator-metal phase transition. A similar behavior, but much weaker, is observed for the band centered at about 580 cm^{-1}. Interestingly, since hardening is associated with a shorter bond and softening with a longer one, this is the spectroscopic expected counterpart of a bond change at the insulator-metal transition suggesting a possible crossover from small to large polarons.[21]

An incipient Drude term is found at 110 K and, at 77 K, the number of carriers shows that $Tl_{1.94}Mn_2O_{6.96}$ is to be considered a poor metal oxide. As Table I shows the plasma frequency is at about 1680 cm^{-1}. Then, from Eq. (4), we calculate an effective carrier number N^* of only $\sim 1:10^{18}$ (we have used an effective electron mass of $\sim 8m_0$). It is to note that we choose for the plasma frequency a fit upper limit because it is known that the granular composition of ceramics, relative to single crystals, lowers the intrinsic specular reflection of a compound. In our spectra this results in a less prominent reflectivity spectra that, in turn, when fitted, translates into a lower value for the plasma frequency.

The imaginary part of the reciprocal dielectric function peaking at longitudinal modes, $-\mathrm{Im}(1/\varepsilon)$, and the real part of the optical conductivity, $\sigma_1=(\omega/4\pi)\varepsilon_2$ (ε_2 is the imaginary part of the dielectric function), Fig. 4, show that the overall effect of the temperature is only significant below T_C. It is also important to note the progressive screening by carriers of longitudinal optical modes when cooling below the phase transition and, in particular, in the region assigned to bending modes. This last point may indicate to the undergoing phase transition directly involving bonds in the octahedral planes since those deformation modes are particularly affected by ion motions in the planes that, in turn, might be indicative of a dynamical anisotropy.

At higher frequencies, the persistence of the band profile

TABLE I. Fitting parameters for $Tl_{1.94}Mn_2O_{6.96}$.

T (K)	ε_∞	Ω_{TO} (cm^{-1})	Ω_{LO} (cm^{-1}) Ω_{pl} (cm^{-1})	γ_{TO} (cm^{-1}) γ_0 (cm^{-1})	γ_{LO} (cm^{-1}) γ_{pl} (cm^{-1})	S_j (cm^{-2})
		93.2	102.2	7.6	7.2	9.934
		119.4	130.7	7.5	11.6	5.776
		161.8	184.1	70.4	193.2	9.148
		185.4	209.2	812.5	231.1	0.298
		275.4	279.7	23.3	12.2	3.338
		285.1	405.5	174.4	131.3	4.119
300	1.78	414.1	422.1	61.1	728.8	0.208
		424.5	484.9	374.6	27.1	0.114
		498.4	519.3	16.5	26.2	0.130
		542.3	613.8	34.5	180.0	0.356
		634.5	660.2	537.7	31.3	0.148
		673.1	943.7	124.6	1752.9	0.144
		94.1	102.2	3.8	7.1	8.467
		119.4	130.9	5.7	9.7	5.828
		161.5	184.1	72.2	214.3	8.708
		185.4	209.2	670.3	208.2	0.279
		274.8	279.1	17.5	10.1	3.202
		284.3	405.5	179.1	128.0	3.811
140	1.65	414.1	422.1	60.0	698.7	0.196
		424.5	487.0	376.9	23.5	0.108
		502.4	525.9	16.6	20.1	0.152
		545.1	615.2	27.0	141.0	0.280
		634.5	661.5	488.7	25.4	0.126
		675.0	943.7	103.3	1780.7	0.130
		94.1	102.2	4.7	13.7	10.281
		119.4	130.7	7.2	24.2	6.925
		161.8	184.1	84.6	273.3	10.67
		185.4	209.2	928.6	172.2	0.345
		273.9	278.9	14.1	9.7	3.145
		287.8	395.1	182.5	89.1	5.453
110	1.55	410.6	411.5	50.7	367.2	0.439
		411.9	488.0	174.8	21.3	0.214
		504.5	526.8	15.1	15.92	0.206
		545.6	607.1	22.0	163.9	0.337
		656.2	660.5	109.6	10.4	0.191
		672.4	1157.5	677.3	2063.8	0.614
			523.8	1261.8	771.6	
		96.1	108.2	6.2	18.4	11.220
		120.4	123.7	6.1	34.9	1.675
		155.8	184.1	108.2	615.7	10.989
		184.4	209.2	618.5	204.3	0.338
77	1.21	272.2	277.9	11.4	16.8	4.785
		280.9	385.1	978.9	333.2	2.401
		414.5	449.5	58.0	22.9	0.979
		451.0	494.8	24.8	19.4	0.052
		505.1	534.8	12.5	17.5	0.125
		549.4	555.0	15.8	155.8	0.067
		599.2	679.8	230.33	11.3	0.853
		715.9	1284.9	454.4	2298.8	0.465
			1680.6	5577.6	4495.6	

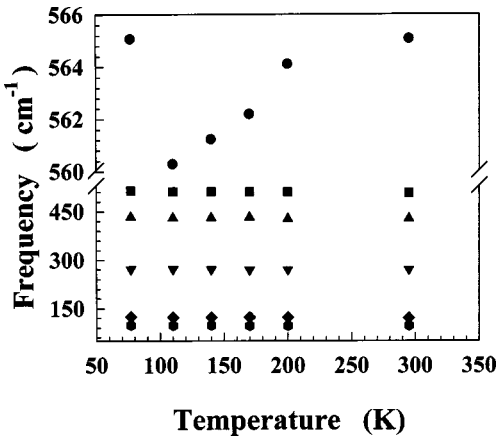

FIG. 3. Temperature dependence of the reflectivity main band peak positions of $Tl_{1.94}Mn_2O_{6.96}$.

between 715 and 1284 cm^{-1}, below T_C, Table I, shows that the would-be mobile carriers remain partially localized and, by the same token, suggests that they would be easily removed from the breathing mode trapped configuration by an external magnetic field.

OPTICAL CONDUCTIVITY

As pointed out above in order to understand the conducting mechanism of $Tl_{1.94}Mn_2O_{6.96}$ we also calculated the temperature dependent optical conductivity using Reik's small polaron theory[16] and then compare these results with those deduced from the dielectric simulation. Between 700 and 1200 cm^{-1} we expect a mixture of contributions due to polarons and to the two-phonon density of states.

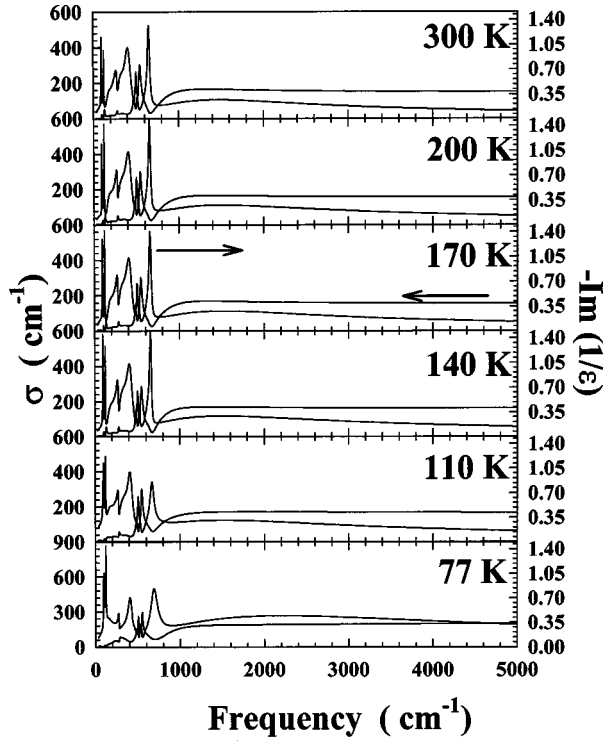

FIG. 4. Temperature dependence of σ_1, the real part of the optical conductivity, and Im$(1/\varepsilon)$, the imaginary part of the dielectric function inverse of $Tl_{1.94}Mn_2O_{6.96}$.

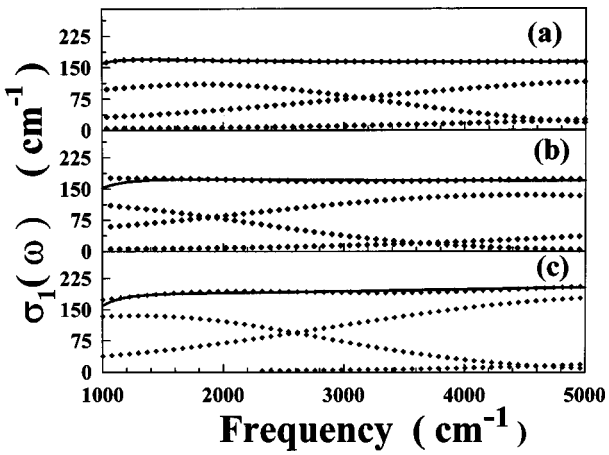

FIG. 5. Optical conductivity of $Tl_{1.94}Mn_2O_{6.96}$. Full lines upper traces are optical conductivities drawn from reflectivity spectra. The superposing diamonds are estimates using Reik's small polaron theory (Refs. 15 and 16). Individual Gaussians correspond to the different phonon contributions (see text). The shown behavior continues asymptotically up to 10 000 cm^{-1}; (a) 140 K, (b) 110 K, and (c) 77 K.

In our analysis we allow, $\overline{\omega}$, the average frequency, and η, characterizing the strength of the electron-phonon interaction, to vary freely in the fit. We compare these results with frequency-dependent experimental data. We found that to cover the complete spectral range up to 10 000 cm^{-1} one simply needs to consider three independent contributions (no correlation between the terms) of the type described in Eq. (5). For our results (Fig. 5), as suggested in Ref. 19, it is only necessary to take into account the highest vibrational band, $\overline{\omega} \sim 650\,cm^{-1}$, assigned to breathing phonons. The result is in very good agreement with the experimental average from transverse and longitudinal optical frequencies taken from Table I and given in Table II between brackets. In this case the calculated fitted frequencies at $\sim$1040.0 cm^{-1} and $\sim$1729.8 cm^{-1} are assigned to overtone and third-order-sum processes, respectively. The number of phonons that form the polaron cloud, ηj $(j=1,2,3)$ is interpreted as for a rather weak electron-phonon interaction. In oxides typical values are in the range $5<\eta<10$ (Ref. 22). The small polaron binding energy is given by $E_b \leqslant \overline{\omega}\,\eta/2$ (Refs. 15 and 16), i.e.,$\sim$ 192 meV at 140 K; $\sim$144 meV at 110 K, and $\sim$169 meV at 77 K showing the persistence below T_C of some trapped polarons coexisting with more delocalized carriers. Those values are in agreement with the preliminary assignment given above for the dipole between 715 and 1285 cm^{-1} in the dielectric simulation. At the same time it suggests that the better conductivity at lower temperatures be achieved by delocalization allowing electron hopping more efficiently due to the ferromagnetic spin alignment.

Then, although with less mobile carriers, the picture emerging from these optical measurements is related to those reported for manganites. As suggested by the reflectivity spectra the changes at about T_C are according to what it is expected from susceptibility and resistivity measurements (Fig. 1) and that the issuing mechanism is singular to the phase transition. The well-defined phonon bands at low temperature reflectivity also suggest that the process is taking

TABLE II. Parameters of the small polaron theory for $Tl_{1.94}Mn_2O_{6.96}$. The values between brackets are phonon frequency averages from a multioscillator fit to experimental reflectivities at their respective temperatures (Table I).

T (K)	η_1	ϖ_{ph1} (cm^{-1})	η_2	ϖ_{ph2} (cm^{-1})	η_3	ϖ_{ph3} (cm^{-1})	ρ^a (Ω cm)
140	4.8	640.1 ⟨648⟩	6.92	1135.0	4.3	1816.4	0.0446
110	3.5	660.0 ⟨658⟩	6.13	1020.1	5.79	1726.1	0.0120
77	4.2	616.0 ⟨639⟩	7.38	967.0	7.88	1647.0	0.0059

[a]Resistivity from measurements shown in Fig. 1.

place at a minority of lattice centers. In contrast with perovskite manganites, where the phonon band structure in the metallic phase is only weakly delineated,[23] the profiles in the spectrum of $Tl_{1.94}Mn_2O_{6.96}$ at 77 K shows that the bulk remains an insulator. Then, the appearance of mobile carriers near T_C reveals the onset of a partial insulator-metal transition in which oxygen defects and lattice distortion due to Tl vacancies may play a role leading one to think that the understanding of the semiconducting behavior of $Tl_{1.94}Mn_2O_{6.96}$ above T_C is related to defects. This may be related to the presence of a significant number of Tl vacancies [0.06(1) atoms per formula unit: it should be recalled that the large electronic conductivity of $Tl_2Mn_2O_7$ is thought to be achieved through the mixing of the voluminous Tl $6s$ orbitals with Mn $3d$ orbitals, in contrast with other insulating $A_2Mn_2O_7$ (A=rare-earths, Sc, In) pyrochlores]. The reduction in the concentration of Tl atoms introduces a strong-scattering $6s$ vacancy into the Tl-O network. Below T_C, the long range ferromagnetic ordering of Mn^{4+} spins leads to a reduction of the spin-scattering fluctuations, giving rise to the observed metallic behavior (with ''poor-metal'' characteristics, as commented before).

We note that although the Mn^{4+} superexchange interaction was found[11] to stabilize the ferromagnetic phase it cannot account for lattice distortions[24] as it is inferred in the broadening below T_C of the band assigned to octahedra symmetric stretching mode (breathing oxygen displacements) (inset, Fig. 2). Our approach is in agreement with $In_2Mn_2O_7$ that with the ferromagnetic ordering at $T_C \sim 120$ K remains an insulator at both ends of this phase transition.[12] It also reflects the overall conclusion pointing the source of the CMR to high incoherent scattering.[11] Here, the infrared spectra working resolution ($\sim$0.25–0.50 meV) brings up local structure arguments that otherwise may go overlooked.

On the other hand, the introduction of ion doping in small quantities is expected to increase the electron scattering centers increasing spin misalignment, and thus, the resistivity. The spin order would be regained when an external magnetic field is applied resulting in a net enhancement of the colossal magnetoresistance.

CONCLUSIONS

Concluding, we have measured the reflectivity and transmission of well characterized samples of $Tl_{1.94}Mn_2O_{6.96}$ between 30 and 10000 cm^{-1}. We found that between room temperature and T_C is an insulator with antiresonances near the longitudinal optical modes indicating distinctive electron-phonon interactions. Below the insulator-metal transition it becomes a poor metal oxide from which we infer the understanding of the colossal mangnetoresistance in pyrochlores is related to the explanations given for manganites. As pointed out by Goodenough[25] for $Ln_{0.7}A_{0.3}MnO_3$ manganites, the overall picture is that of small mobile polaron holes (electrons in pyrochlores) trapped with decreasing temperature (this is reflected in the need of an infrared dipole at 673–943 cm^{-1} in the dielectric simulation, Table I, and the sharpening of the band profile centered 1000 cm^{-1} in going from 300 to 140 K) and then released with decreasing temperatures below T_C (that in our infrared spectra shows as antiresonance smoothing, in particular, the feature at 670 cm^{-1} and phonon screenings like those at about 180 cm^{-1}) all in an apparent single crystallographic phase.

We also found an excellent agreement between the experimental and the calculated, using Reik's small polaron theory, optical conductivity strongly suggesting that conductivity in $Tl_{1.94}Mn_2O_{6.96}$ be achieved by phonon assisted electron hopping.

ACKNOWLEDGMENTS

This research has been partially supported by Grant No. PICT 8017 of the National Research Council of Argentina (CONICET). Financial support by the Spanish CICYT (Comisión Interministerial de Ciencia y Tecnologia) under Project No. PB97-1181 is also acknowledged.

*Electronic address: nem@dalton.quimica.unlp.edu.ar

[1] M. A. Subramanian, G. Aravamudan, and G. V. Subba Rao, Prog. Solid State Chem. **15**, 55 (1983).

[2] C. Zener, Phys. Rev. **82**, 403 (1955).

[3] G. H. Jonker and J. H. Van Santen, Physica (Amsterdam) **XVI**, 337 (1950).

[4] Guo-meng Zhao, M. B. Hunt, and H. Keller, Phys. Rev. Lett. **78**, 955 (1997).

[5] A. J. Millis, B. Y. Shraiman, and R. Mueller, Phys. Rev. Lett. **77**, 175 (1996).

[6] Y. Shimikawa, Y. Kubo, T. Manako, Y. V. Suchko, D. N. Argyriou, and J. D. Jorgensen, Phys. Rev. B **55**, 6399 (1997).

[7] Y. Shimakawa, Y. Kubo, and T. Manako, Nature (London) **379**, 53 (1996).
[8] Traces of high pressure synthesis residues, Tl_2O_3 and MnO_2, may be considered as extrinsic impurities of $Tl_2Mn_2O_7$.
[9] M. A. Subramanian, B. H. Toby, A. P. Ramirez, W. J. Marshall, A. W. Sleight, and G. H. Kwei, Science **273**, 81 (1996).
[10] H. D. Rosenfeld and M. A. Subramanian, J. Solid State Chem. **125**, 278 (1996).
[11] G. K. Kwei, C. H. Booth, F. Bridges, and M. A. Subramanian, Phys. Rev. B **55**, R688 (1997).
[12] S.-W. Cheong, H. Y. Hwang, B. Batlogg, and L. W. Rupp, Jr., Solid State Commun. **98**, 163 (1996), and references therein.
[13] T. Kurosawa, J. Phys. Soc. Jpn. **16**, 1208 (1961).
[14] F. Gervais, J. L. Servoin, A. Baratoff, J. G. Bednorz, and G. Binnig, Phys. Rev. B **47**, 8187 (1993).
[15] H. G. Reik and D. Heese, J. Phys. Chem. Solids **28**, 581 (1967).
[16] H. G. Reik, in *Polarons in Ionic Crystals and Polar Semiconductors*, edited by J. Devreese (North-Holland, Amsterdam, 1972).
[17] R. Kubo, J. Phys. Soc. Jpn. **12**, 570 (1957).
[18] T. Holstein, Ann. Phys. (N.Y.) **8**, 343 (1959).
[19] R. Mühlstroh and H. G. Reik, Phys. Rev. **162**, 703 (1967).
[20] N. E. Massa, J. A. Alonso, M. J. Martinez-Lope, and Y. Z. Casais (unpublished).
[21] See, for example, S. J. L. Billinge, R. G. DiFrancesco, G. H. Kwei, J. J. Neumeier, and J. D. Thompson, Phys. Rev. Lett. **77**, 715 (1996). Also, A. Lanzara, N. L. Saini, M. Brunelli, F. Natali, Bianconi, P. G. Radaelli, and S.-W. Cheong, *ibid.* **81**, 878 (1998).
[22] H. G. Reik, Z. Phys. **203**, 346 (1967).
[23] K. H. Kim, J. Y. Gu, H. S. Choi, G. W. Park, and T. W. Noh, Phys. Rev. Lett. **77**, 1877 (1996).
[24] J. B. Goodenough, Phys. Rev. **100**, 564 (1955).
[25] J. B. Goodenough, J. Appl. Phys. **81**, 5330 (1997).